**We thank Journal of Infrared, Millimeter, and Terahertz Waves**
The final publication is available at Springer via
http://dx.doi.org/10.1007/s10762-016-0331-4

# High efficiency wideband refractive optics for ALMA Band-1 (35-52 GHz)

## Design, implementation and measurement results

**V. Tapia · A. González · R. Finger · F. P. Mena · D. Monasterio · N. Reyes · M. Sánchez · L. Bronfman**

Received: 3 May 2016 / Accepted: 13 October 2016

**Abstract** We present the design, implementation and characterization of the optics of ALMA Band 1, the lowest frequency band in the most advanced radio astronomical telescope. Band 1 covers the broad frequency range from 35 to 50 GHz, with the goal of minor degradation up to 52 GHz. This is, up to now, the largest fractional bandwidth of all ALMA bands. Since the optics is the first subsystem of any receiver, low noise figure and maximum aperture efficiency are fundamental for best sensitivity. However, a conjunction of several factors (small cryostat apertures, mechanical constraints and cost limitations) makes extremely challenging to achieve these goals. To overcome these problems, the optics presented here includes two innovative solutions, a compact optimized-profile corrugated horn and a modified Fresnel lens. The horn profile was optimized for optimum performance and easy fabrication by a single-piece manufacturing process in a lathe. In this way manufacturability is eased when compared with traditional fabrication methods. To minimize the noise contribution of the optics a one-step zoned lens was designed. Its parameters were carefully optimized to maximize the frequency coverage and reduce losses. The optical assembly reported here fully complies with ALMA specifications.

**Keywords** Horn antenna · dielectric lens antenna · optics

V. Tapia · R. Finger · D. Monasterio · M. Sánchez · L. Bronfman
Astronomy Department, Universidad de Chile
Camino El Observatorio 1515, Las Condes, Santiago, Chile
Tel.: +562-2-9771119
E-mail: valeria.tapia@raig.uchile.cl

N. Reyes · F. P. Mena
Electrical Engineering Department, Universidad de Chile
Av. Tupper 2007, Santiago Centro, Santiago, Chile

A. González
National Astronomical Observatory of Japan, Tokyo, Japan
2-21-1 Osawa Mitaka, Tokyo 181-8588

## 1 Introduction

The Atacama Large Millimeter/Submillimeter Array (ALMA) [1] is a gigantic revolutionary interferometry radio telescope constructed by international partnership. Such consortium includes the collaboration of Europe, North America, East Asia and Chile. ALMA consists of 66 Cassegrain antennas, with a total collecting area of 5650 $m^2$. The antennas can be placed in different configurations, allowing baselines of up to 16 km and an angular resolution of 5 milliarcseconds in the most extended configuration and highest frequency. Each antenna is designed to cover the frequency range from 35 to 950 GHz using 10 dual linear-polarization heterodyne receivers [1][2]. At the moment of writing, the receivers that cover frequencies above 84 GHz have been or are being integrated inside the cryostat of every antenna.This paper describes the design, optimization, fabrication, and verification of the optical system of the first band of ALMA (35–52 GHz). To comply the stringent technical specifications [3] the design incorporates two innovative components, an optimized-profile corrugated horn in combination with a modified zoned lens.

## 2 The band 1 receiver

The Band-1 heterodyne receiver [4][5] is a dual-polarization single-side-band receiver that covers the frequency range from 35 to 50 GHz, with the goal of extending the coverage to 52 GHz in a best-effort basis. The receiver can be divided into three subsystems: optics, amplification and down-conversion.

The RF signal collected by the Cassegrain antenna is refocused, by a lens placed near the antenna secondary focus, onto a horn antenna located inside the cryostat. The optics should also include a cryostat window, providing the vacuum seal. The RF signal goes through two infrared filters along its way between the optics and the horn in the receiver. The signal captured by the horn is then divided into two orthogonal linear polarizations by means of a waveguide ortho-mode transducer. The two resulting signals are then amplified by state-of-the-art low-noise amplifiers and down-converted to a 4-12 GHz intermediate frequency (IF) by room-temperature mixers. Finally, the two IF signals are filtered and amplified in order to condition them for processing at the telescope back end. To minimize the noise introduced by the receiver each subsystem has to be optimized, in particular those at the beginning of the receiving chain. Since the optics is the first subsystem, optical losses affect all other noise terms in the receiver. Therefore, apart from good aperture efficiency, optics must have low loss and low noise temperature.

### 2.1 Requirements on the optics

The optics of the ALMA Band-1 receiver combines a series of stringent technical specifications, construction constraints and cost limitations that require

**Table 1** Band-1 requirements for the optical system.

| Feature | Requirement |
|---|---|
| Frequency range | 35-50 GHz, goal is up to 52 GHz |
| Aperture efficiency | Larger than 80% |
| Polarization efficiency | Larger than 99.5% |
| Noise temperature | Lower than 10 K (Not ALMA spec) |
| Angular misalignment | Lower than 5 mrad |
| Mechanical concerns | No mechanical tuning |
| | No interference with existing devices |
| | 7-m and 12-m antennas adaptability |

trade-offs. The main specifications for the optical system are the following. The RF frequency range is 35–50 GHz (35.3% of bandwidth), with the goal of extending the coverage to 35–52 GHz (39.1% of bandwidth). It must meet a total aperture efficiency at the sub-reflector that exceeds 80% including spillover, amplitude, phase, defocus and polarization efficiencies. The polarization efficiency must be better than 99.5%, which corresponds to an integrated cross-polarization signal over the secondary of less than $-23$ dB relative to integrated co-polar power on secondary. It is preferred that the illumination provided by the optical system is frequency independent across the band. The maximum total noise for the Band-1 receiver must be less than 25 K over 80% of the band and 32 K over 100%. Receiver noise budgets show that the maximum noise contribution from the optics must be around 10 K. Regarding mechanical considerations, the optics cannot interfere with the already-existing devices or the optical systems for other bands. Moreover, an angular alignment of the optical beam within 5 mrad of its nominal direction should be attained without mechanical tunings. Finally, the same receiver design must be used for the 7-m and 12-m antennas, even though the angle at which the secondary is seen by the receiver is different in each case. A summary of these requirements is shown in Table 1.

## 3 Horn antenna

Standard conical profile corrugated horns achieve the high performances required for radio astronomy by increasing their length and using narrow flare angles. This makes fabrication by direct machining in a single block difficult, and forces the use of other techniques which are either not appropriate or complex (e.g. split block, electroforming or direct machining of several metal rings to be assembled together). These later alternatives can be time consuming and relatively expensive when dozens of units are needed. Moreover, conical corrugated horns can be too long and bulky to be included in the limited space within a cryostat. For these reasons, an optimized-profile corrugated horn is more appropriate for ALMA Band-1 receivers. Such a horn can be directly machined as a single piece on a CNC lathe if some mechanical constraints are included in the optimization process.

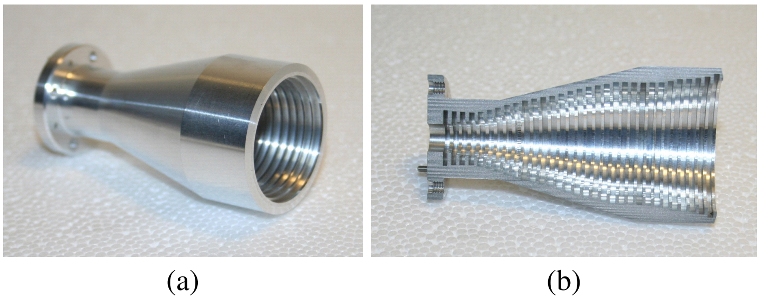


**Fig. 1** Optimized-profile corrugated horn. (a) Constructed horn. (b) Cross-section view of a sacrificial horn. The overall length of the horn is 70 mm.

### 3.1 Design

The profile of the horn was designed using mode-matching (MM) software, Microwave Wizard [6], with a genetic algorithm for optimization. The optimization parameters are the number of corrugations and the width, depth and teeth-slot pitch of each corrugation. Additional restrictions to the problem are the maximum corrugation depth, 3.2 mm to provide enough space for the cutting tools, and the total horn length, shorter than 80 mm to avoid tool vibrations during fabrication. If an appropriate horn profile is used, the beam pattern can be up to 99% fundamentally Gaussian [7]. Moreover, special attention was given to the optimization of the first six corrugations next to the input waveguide. These corrugations correspond to the converter mode and provide the necessary impedance matching to transform the $TE_{11}$ mode of the input circular waveguide into the $HE_{11}$ hybrid mode propagating into the horn [8]. A combination of variable-depth and variable-pitch-to-width mode converters was used. This strategy allows adding flexibility in the design without increasing the corrugation depth beyond the intended fabrication limits [9]. The characteristics of the ideal Gaussian feed were determined by optimizing a quasi-optical model of the Band-1 optics. According to it, a beam-waist of about 9.4 mm is required to achieve frequency independent illumination while minimizing truncation through the window of the cryostat and the holders of the infrared filters. An initial profile of aperture $0.64 \cdot w$, input waveguide radius 6.7 mm and corrugation with linear depth decreasing from $\lambda_c/2$ to $\lambda_c/4$ was created. Based on previous experience some corrugations were modified to improve this initial model. In particular, the shape of the mode-converter section and corrugations near the aperture were modified, the former increasing the depth and the latter forming a launcher. This initial profile was optimized to provide the intended Gaussian patterns and achieve low cross-polarization and waveguide input return loss, less than $-35$ dB and $-30$ dB, respectively. Moreover, different optimization goals were used to force a good symmetry of the radiation patterns across the RF band. The difference in phase-center

**Table 2** Mechanical parameters of the corrugated horn antenna

| Feature | Requirement |
|---|---|
| Input waveguide radius | 3.35 mm |
| Aperture radius | 15.63 mm |
| Total length | 70 mm |
| Number of corrugations | 31 |
| Width of the corrugations | 0.80–0.93 mm |
| Width of the gap | 1.06–1.35 mm |
| Depth of corrugations | 2.84–1.50 mm |

location (PCL) and the 10-dB beamwidth between the E and H planes were set to be smaller than 0.5 mm and 0.1°, respectively. Using these goals, an optimal horn design was achieved. It has 31 corrugations and a length of 70 mm. Its main mechanical parameters are shown in Table 2. The resulting profile is compact, with a length of 10 wavelengths at the central frequency of ALMA Band 1. The profile does not follow any simple known function and would be better expressed by an approximation of splines. The corrugations are less deep than a standard horn and present smooth changes, less than 0.6 mm, between two correlative corrugations. This provides a good impedance match to propagate the modes that comply the hybrid condition [10]. The designed horn was validated using HFSS Finite Element Method solver [11] on frequency domain bases. Reflection losses and far-field radiation patterns from HFSS and MWW were compared and generally showed good agreement.

### 3.2 Horn fabrication and characterization

Several horns were fabricated from a single block of aluminum in a CNC lathe, as shown in Figure 1. One of the horns was sacrificed to test the fabrication procedure, which was rendered within tolerances. The repeatability of the fabrication process was further assessed from the reflection losses at the circular input waveguide of several horns. For this measurement the horn aperture was terminated with an absorber located a few centimeters in front of the aperture. A comparison between simulated and measured values is shown in Figure 2. The measured reflection losses are better than 26 dB over the complete band of interest, in agreement with electromagnetic simulations.

One of the horns was characterized in a near-field planar beam-pattern scanner built specifically for this work. The complete setup was enclosed within absorbers in order to provide an anechoic environment. It was assembled in an optical table in order to ensure the correct position, angle and alignment of all the components. The setup, shown in Figure 3a, is based on a 50-GHz Network Analyzer and a $XY\theta$ scanner. The XY plane perpendicular to the optical axis was sampled until the first side lobe. To meet the Nyquist criterion the separation of measured points was $0.48\lambda$. After the measurement was completed, the measured near-field data was transformed into far-field data using an algorithm based on the Fourier Transform.

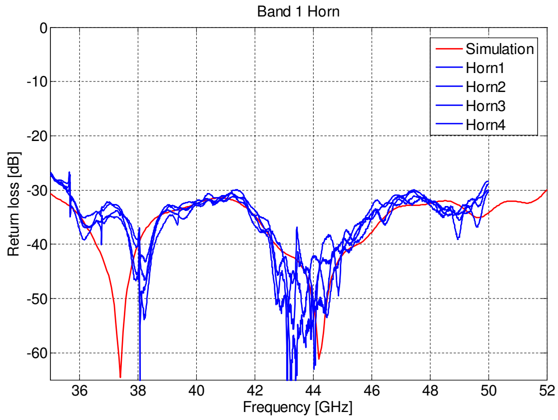


**Fig. 2** Measured and HFSS-simulated reflection losses of the horn antenna. All the curves have a resolution of 50 MHz. Four different horn measurements are presented, showing the excellent repeatibility.

Figure 3b shows a comparison between measured and simulated far-field radiation patterns. They are identical up to 20 dB, with minor differences at the level of the side lobes. The horn meets the designed beam-waist, has low side-lobes, cross-polar better than −30 dB and symmetric patterns between the E and H planes.

## 4 Focusing system

Different solutions based on mirrors and lenses were studied [12][13]. Mirrors are preferable since they present lower loss than dielectric lenses. Nevertheless, a solution with mirrors was not possible with the existing mechanical restrictions. Consequently, a lens-based configuration was selected, as otherwise recommended in the original ALMA-receiver optics design [2],[14].

### 4.1 Initial lens design

A quasioptical analysis indicates that if a single cold lens was used, the beam would be strongly truncated in the cryostat apertures [12]. Hence, a warm lens is required. Two configurations have been studied, a system including a single warm lens and a system composed of a cold and a warm lens. The best configuration was the single warm lens. If two lenses are used, the warm lens must be large enough to appropriately refocus the beam, resulting in the same or greater signal loss than the single lens configuration. Moreover, the warm lens can be used as vacuum window if an appropriate material is chosen and some mechanical constraints are taken into account. Different materials have been considered: quartz, fused silica, sapphire, PTFE and HDPE. The decision was made considering the dielectric constant, loss tangent, mechanical characteristics and ease of fabrication. Although quartz, fused silica and sapphire, on the

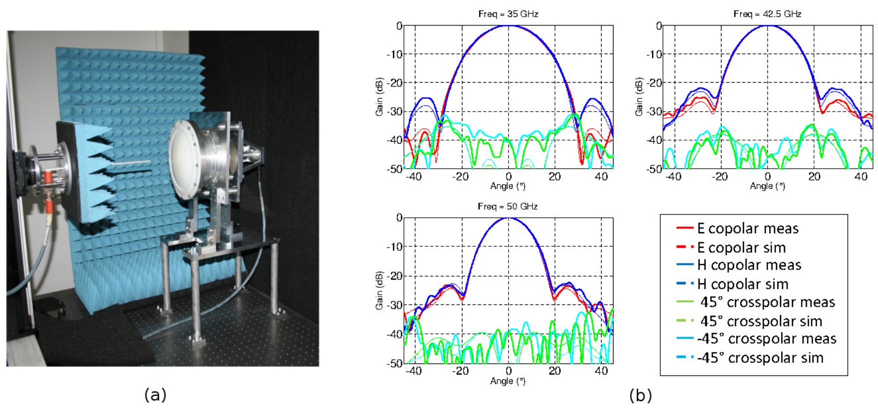


**Fig. 3** (a) Near-field beam scanner setup with the complete Band-1 optical system. The same setup was used to test the horn alone.(b) Measured and HFSS-simulated far-field patterns at 35, 42.5 and 50 GHz for the spline corrugated horn.

one hand, have high dielectric constant, implying a thinner lens, adding antireflection (AR) layers is more complex and reduces the bandwidth. HDPE and PTFE, on the other hand, have low dielectric constant, relatively low loss tangent, and are plastic materials which eases lens and AR coating fabrication. Common methods like lathe milling or injection molds can be used. HDPE was chosen over PTFE because it exhibits less creep deformation. Therefore, a single HDPE warm-lens configuration was selected for further optimization.

A bi-hyperbolic lens, as the one considered for ALMA Band 1, has three design parameters: diameter; thickness of the central slab between the hyperbolic curves on each side of the lens; and focal length. The diameter was set to the maximum possible, 190 mm, to minimize truncations of the lens without interfering with existing antenna hardware. The diameter of the lens is a highly relevant parameter since it determines the maximum efficiency that the system can achieve. The incoming radiation from the Cassegrain antenna can be approximated at the lens aperture by an Airy pattern determined by the size of the secondary mirror, since it is close to the Cassegrain secondary focus [3]. Considering a 190-mm-diameter lens, the maximum power admitted into the cryostat, and which represents the maximum achievable aperture efficiency, is between 84% at 35 GHz and 90% at 50 GHz [13]. The thickness of the lens central slab was set to 8 mm, which is the required thickness for supporting the pressure difference with a safety factor of 5 [15]. The focal length and the position of the lens were initially calculated with a quasi-optical model. Best results were obtained with a lens located at a distance of 175.2 mm from the horn aperture and a focal length of 168 mm. If a standard bi-hyperbolic lens is used, the resulting lens is thick, measured in wavelengths, with an added noise temperature of about 13 K, where 7.5 K comes from the dielectric loss in the material. The thickness of the lens can be reduced if a Fresnel zone

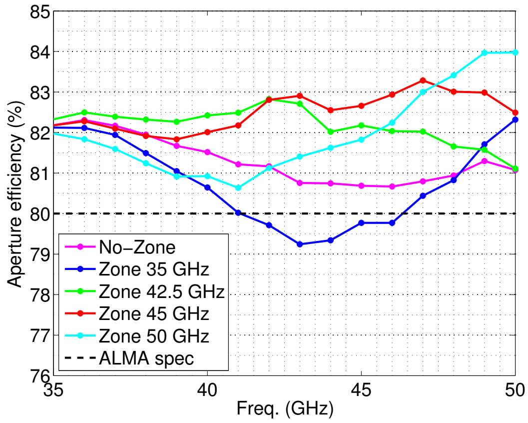


**Fig. 4** Comparison of simulated aperture efficiencies obtained for lenses with zones designed at different frequencies. A lens without zone has also been included in the comparison.

is introduced [16]. This gives two new design parameters, the position of the zone and the frequency at which the profile of the zone is calculated. Our strategy was to place the zone at the outer area of the lens minimizing reduction on the system bandwidth. Considering a quasioptical approach, at high frequencies, where the beam size is smaller, the zone will not be seen by the main beam. Nevertheless, a more complex analysis, were high-order mode effects are included, show that the aperture efficiency is affected. At lower frequencies, the zone will have a mayor effect but it was optimized to minimize aperture-efficiency losses. The zone was designed considering that the difference in optical paths for a ray in the central hyperbola and for the one in the zone equals $2\pi$. This condition can only be met at the design frequency of the zone. Additionally, the discontinuous surface may produce some shadowed areas in the outer surface which degrade performance. These effects were assessed with further simulations described in the next subsection.

To complete the initial design of the lens, an antireflection structure was studied to compensate for the difference in relative permittivity between HDPE and air. This is important due to the fact that most of the radiation is concentrated in the center of the lens, where the faces are almost parallel. Therefore, to minimize reflective losses and standing waves inside the lens and between lens and other components, a corrugated surface was included in both sides of the device. The dimensions of the corrugations were designed at the central frequency using a transmission-line equivalent analysis [17]. The calculations resulted in corrugations with thickness of 1 mm, pitch of 2 mm, and an average depth of approximately 1.42 mm.

## 4.2 Lens-profile optimization and full-system simulations

The effects of changing the zone and AR-structure parameters were analyzed using full-wave Method-of-Moments (MoM) analysis. The final optical design and optimization were performed with WaspNET [18], which implements an

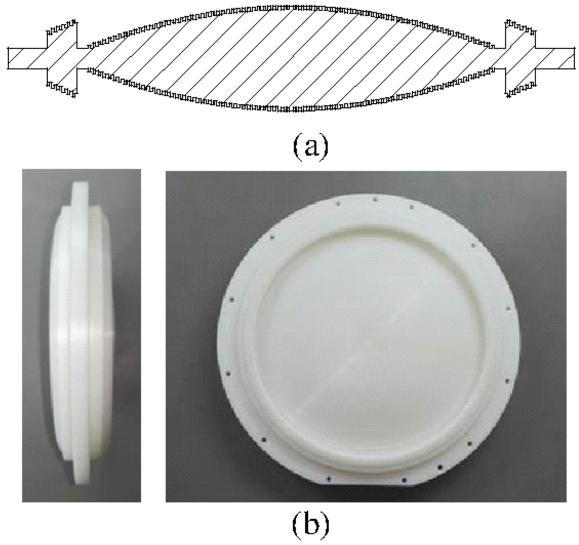

**Fig. 5** Zoned-lens for ALMA Band-1 optics. (a) Profile of the lens. (b) Lateral and upper views of the fabricated lens. Its outer diameter is 220 mm.

hybrid mm/MoM code. This allows to simulate the horn and the zoned lens (including its metal support structure) simultaneously, taking into consideration all electromagnetic effects between them. The speed of simulations was increased by using the Body of Revolution MoM code in this software. Under these conditions, the simulation of the full optical system required around 7 minutes per frequency point in a powerful 16-CPU computer. This simulation speed allowed to perform parametric analyses on the different design parameters and to try different lens designs. After far fields had been calculated with WaspNET, they were used to calculate the efficiencies at the ALMA antenna secondary mirror. Results were obtained at several frequencies and compared for different designs. Besides the bi-hyperbolic lens, a plane-hyperbolic one was also studied. However, the best results in terms of aperture efficiency were obtained for a bi-hyperbolic lens with a focal length of 180 mm and a distance between horn and lens central point of 175.4 mm.

The position of the zone and frequency of design were carefully chosen with full-wave simulations and the focal length and position of the lens were re-tuned. After various parametric analyses, several candidate designs were chosen and simulated with a fine-frequency sweep in order to decide on the final optical design. A comparison between zones designed at different frequencies and a lens without a zone is shown in Figure 4. It can be noticed that the zone introduces frequency dependence, strongly changing the structure of the curves and improving the efficiency especially near to the designed frequency. Moreover, comparing the zoned and no-zoned lenses, we can see that if we properly select the frequency of the zone, we can obtain better aperture efficiency. This counterintuitive effect is originated in the fact that high-order modes are constructively coupled at the illuminated surface. The best result was found for the 45-GHz zoned lens, presenting a balanced level of efficiency

**Fig. 6** Comparison between results using HFSS and WaspNET. Difference on total efficiency between the two approaches is in the order of 1%.

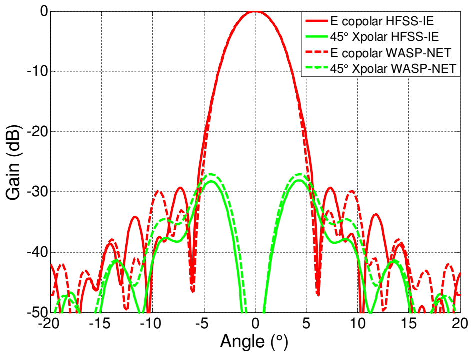


across the band. Finally, some slight modifications were implemented on the lens profile in order to ease fabrication and to reduce the thickness as much as possible without degrading the optical performance. In particular, the hyperbolic profiles of the lens have been approximated by flat steps perpendicular to the axis of revolution. The value of the step is equal to the value of the hyperbola in the middle of the step [13]. Additionally, the outermost corrugations in the central hyperbola have been removed in order to keep the central slab thickness of 8 mm, the minimum possible total lens thickness. These modifications had a minimal impact in the aperture efficiency and resulted in a maximum lens thickness of 40.8 mm. The final profile of the lens is shown in Figure 5. To check the consistency of the results, the full system was cross-simulated using HFSS. Because of the large separation between the lens and the horn, the simulation of the system was divided in two steps. The horn was first simulated and the radiated near fields were calculated. This results were used as excitations for the lens which was simulated using HFSS-IE. A comparison between the two simulation approaches is presented in Figure 6.

Summarizing, the complete system consists of a compact spline-profile corrugated horn machined from a single block of aluminum, a low-loss HDPE one-zone bi-hyperbolic lens, and the holder of the lens including vacuum interfaces as shown in Figure 7. Due to the off-axis location of the Band 1 receiver in the cryostat, the optical axis of the system is tilted by 2.48° with respect to the cryostat axis.

### 4.3 Lens-noise contribution

The total noise contribution was estimated considering all the components in the optical path between the horn and the cryostat. The components considered were the 15-K and 110-K infrared filters, the aperture of the cryostat and the lens. Moreover, we computed the noise added by dielectric losses, truncation and reflections, where some simplifications were deemed in the model. The truncation losses were estimated using a large number of Gaussian higher-order modes, excluding from the model the tilt and the offset in infrared filters.

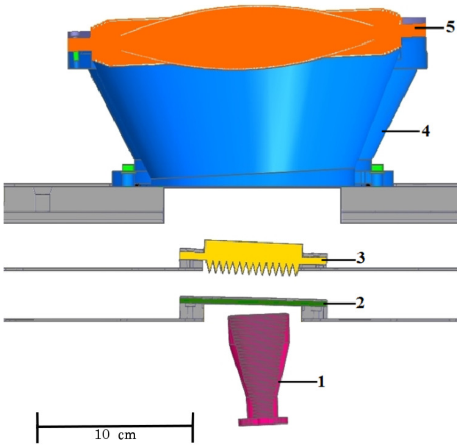


**Fig. 7** Cross-section of the proposed optics for the 12-m antennas. 1: Spline profile horn antenna, 2: 15 K infrared filter, 3: 110 K infrared filter, 4: lens holder, 5: One-zone modified Fresnel lens.

For dielectric losses, the lens was approximated by a dielectric slab with thickness equal to the total lens thickness. In addition, reflection losses in the lens and infrared filters were calculated assuming perfect anti-reflection treatment. Finally, the physical temperature of each component for termination of truncated beams was estimated as the weighted sum of the previous and the next stages in the path. The computed noise temperature of the optical system at different frequencies was estimated between 8.9 and 10.1 K, where dielectric losses contribute 5.6 K in average..

### 4.4 Solution for the 7-m antennas

So far we have described the solution for the 12-m antennas of the ALMA array. However, as mentioned above, the system must also be compatible with the 7-m antennas. These antennas have an angle of projection on the sub-reflector of 4.28° (instead of 2.48° as in the 12-m antennas). To achieve this angle with the same front end, several solutions are possible. One of them is introducing a prism between the lens and the secondary of the antenna. Although the prism contributes to the noise temperature in several kelvins and introduces extra reflection losses, it is easy to handle and does not interfere with the vacuum in the cryostat. Alternatively, the same tilt effect can be achieved by offsetting the lens position. This solution has been implemented here using a different holder for 7 and 12-m antennas, causing no extra noise contribution. In order to produce a deflection of 1.8°, it is necessary an offset of 5.66 mm perpendicular to the axis of propagation. Even if some degradation can be noticed respect to 12-m antennas, HFSS simulations show that aperture efficiency is still higher than 80%.

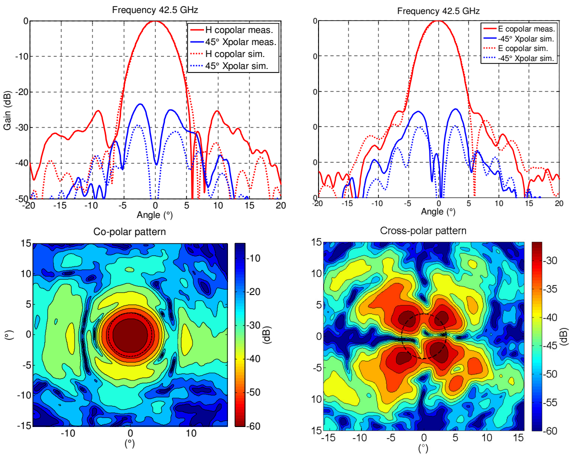


**Fig. 8** Measured and simulated far-field pattern at 42.5GHz for Band 1 optics including cryostat apertures and filters. Top panels shows the E and H patterns along with the cross-polar levels. Bottom panels show the measured co-polar and cross-polar patterns.

### 4.5 Lens fabrication

The lens was built in a CNC lathe, see Figure 5b, using a block of HDPE whose dielectric constant and loss tangent were previously characterized in our laboratory. The characteristics of the used HDPE are critical in the design of the lens, since the dielectric constant affects the focus of the devices and the loss tangent determines the lens noise temperature by dielectric losses. Therefore, twelve samples from different positions and angles of the same HDPE block were measured in a rectangular WR22 waveguide and characterized using a multi-reflection model. The obtained mean values were $\epsilon_r = 2.347 \pm 0.004$ and $\tan\delta = 2.23 \cdot 10^{-4}$. These values were used in all the calculations presented in this paper.

## 5 Full-system measurements

### 5.1 Optics for the 12-m antennas

We have mounted the optical system using a mock-up of the ALMA cryostat where the Band-1 receiver will be placed. This structure ensures the exact position of the components in a realistic situation. It holds the horn, the 15-K and 110-K shields, the cryostat aperture, the holder of the lens and the one-zone Fresnel lens. The infrared filters were not included in order to validate only the optical system presented here, without possible second-order effects not considered in the design. Then, the entire system was characterized in the same near-field planar beam-pattern scanner described in section 3.2. Near-field measurements swept a plane of 50×50 cm, where the distance between the scanner probe antenna and the top of the lens was set to 50 cm.

Figure 8 shows a comparison between simulated and measured far-field radiation patterns at one frequency, showing an excellent agreement. The

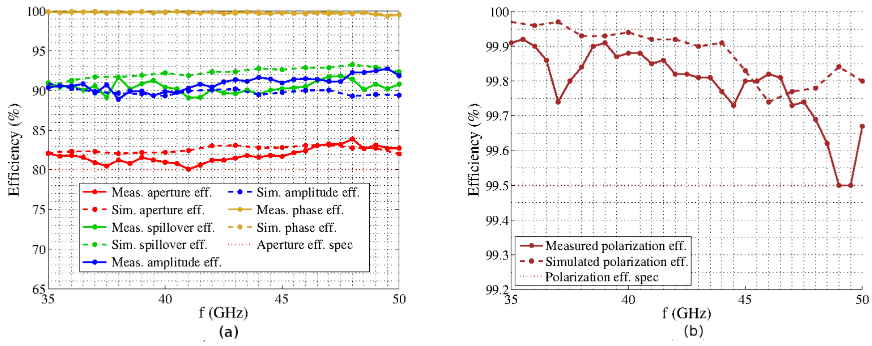


**Fig. 9** Comparison between measured and simulated efficiencies. (a) Aperture, spillover, phase and amplitude efficiency. (b) Polarization efficiency.

patterns exhibit good E and H-plane symmetry, low side-lobes level and cross-polar better than −23 dB. From the measured radiation patterns we calculated the aperture, spillover, phase and polarization efficiencies. In Figure 9 we compare them with the simulated efficiencies. All of them meet ALMA specifications. Nevertheless, some differences can be noticed between the curves. The simulation model in WaspNet did not include the effects of the finite size of the apertures in the cryostat shields. We did not include the shields in the simulation model, since they are large structures and are not centered around the optical axis. The inclusion of these shields would break the Body of Revolution symmetry and increase the computing time dramatically. Another point to consider is that the shields have small apertures. Indeed, the aperture radius of the 110-K shield is just 2.5 times the beam radius. As a result beam truncations are expected at the lower frequency range, producing higher level side-lobes and smaller effective beam radius. Moreover some coupling effects between the apertures and the horn near fields are observed, causing a reduction in total efficiency at some frequencies. One noticeable effect of this effect is the reduction of polarization efficiency at 49 GHz. Accounting for this differences between our simulation procedure and effective measured data we can say that the simulation procedure is accurate enough to predict the performance of the system within a 1% accuracy on total aperture efficiency.

## 5.2 Optics for the 7-m antennas

The measurements were also performed for the solution proposed for the 7-m antennas. In this case the cryostat mock-up contained a lens holder with the appropriate offset. As in the previous section, the results (not presented here for the sake of space) showed an excellent agreement with the simulations.

## 6 Conclusions

We have presented the design, implementation and characterization of the optics for the ALMA Band 1 receiver. We have demonstrated that despite the stringent specifications and strong constrains imposed on the optical system, it fully complies with all ALMA requirements. Over the entire frequency range the measured aperture efficiencies are greater than 80%, the polarization efficiencies are better than 99.5% and the spillover efficiencies better than 89.1%. Moreover, the calculated noise temperature is between 8.9 and 10.1 K. To achieve these results we have used two innovative components, a compact optimized-profile corrugated horn and a modified Fresnel lens. In the case of the horn we have demonstrated that is possible to optimize the profile for both an outstanding performance and a very short electrical length for best manufacturability. For the lens we have demonstrated that a zoned lens produces the required illumination pattern, overcoming the inherent bandwidth limitations that this technique usually causes, and reducing the noise contribution compared with standard bi-hyperbolic lenses.

**Acknowledgements** This work was supported partially by CONICYT grant CATA Basal PFB06; ALMA-CONICYT Project 31120005 and 31150012; FONDECYT projects 11140428 and 11151022; CONICYT Grant AIC-27; QUIMAL fund project 140002; and ESO-Chile Joint Committee. We thank National Instrument for the donation of software licences. Finally, we would like to especially thank Jos Pizarro for his support and manufacturing the horns and the lens used in this paper.

## References

1. A. Wootten, and A. Thompson, The Atacama Large Millimeter/Submillimeter Array, Proceedings of the IEEE, vol.97, 1463 (2009).
2. H. Rudolf, M. Carter, and A. Baryshev, The ALMA Front End OpticsSystem Aspects and European Measurement Results, IEEE Transactions on Antennas and propagation, vol. 55,(2007).
3. James W. Lamb, Low-Noise, High-Efficiency Optics Design for ALMA Receivers, IEEE Transactions on antennas and propagation, vol. 51, N°.8, (2003).
4. J. Di Francesco et al.,The science cases for building a Band 1 receiver suite for ALMA, arXiv:1310.1604v3, (2013).
5. T. Huang et al., "Development of Band-1 receiver cartridge for Atacama Large Millimeter/submillimeter Array (ALMA)," in Proc. SPIE 9153, Millimeter, Submillimeter, and Far-Infrared Detectors and Instrumentation for Astronomy VII, p. 14. (2014)
6. $\mu$Wave Wizardtm, Mician GmbH, software description. Available: http://www.mician.com/
7. R. Gonzalo, J. Teniente, and C. del Ro, Improved Radiation Pattern Performance of Gaussian Profiled Horn Antennas, IEEE Transactions on antennas and propagation, Vol. 50, N°. 11, (2002)
8. J. Graeme L, "Analysis and Design of TE11-to-HE11 Corrugated Cylindrical Waveguide Mode Converters," Microwave Theory and Techniques, IEEE Transactions, vol. 29, N$^{O}$. 10, pp. 1059, 1066 (1981).
9. C. Granet and Graeme L. James, "Design of corrugated horns: a primer," Antennas and Propagation Magazine, IEEE, vol. 47, N°. 2, pp. 76-84 (2005).
10. P.J.B. Clarricoats and P.K. Saha, "Propagation and radiation behaviour of corrugated feeds. Part 1: Corrugated-waveguide fe bed," Proceedings of the Institution of Electrical Engineers, vol. 118, no. 9, pp. 1167-1176, 1971.

11. High Frequency Structure Simulator, Ansys Academic Research, release 15.0.2.
12. N. Reyes, et al., "Design of the optical system for ALMA Band 1," in Proceedings of SPIE Vol. 9145, p. 91451W (2014).
13. A. Gonzalez, et al., "Alternative optics design for the ALMA Band 1 receiver (3552 GHz)," in European Conference on Antennas and Propagation (EuCAP), pp. 1-4 (2015).
14. M. Carter, et al., "ALMA Front-end Optics," ALMA, Design report FEND-40.02.00.00-035-B-REP, (2007).
15. M. Tejada, Fatigue and creep behavior of ALMA Band-1 lens, Millimeter Wave Lab U. Chile, Santiago, Chile, Mech. Rep., (2015).
16. J. L. Volakis (editor), Antenna Engineering Handbook, Chapter 18, 4th Edition, Mc Graw-Hill, (2007).
17. T. Morita and S. B. Cohn, "Microwave lens matching by simulated quarter-wave transformers", IRE Transactions on Antennas and Propagation, vol. 4, no. 1, pp. 33-39, 1956.
18. MIG WASP-NET, software description. Available: http://www.mig-germany.com/